Quantum Spin Torque Driven Transmutation of an Antiferromagnetic Mott Insulator

Marko D. Petrović,[1] Priyanka Mondal,[1] Adrian E. Feiguin,[2] and Branislav K. Nikolić[1,*]
[1]Department of Physics and Astronomy, University of Delaware, Newark, Delaware 19716, USA
[2]Department of Physics, Northeastern University, Boston, Massachusetts 02115, USA

(Received 12 October 2020; accepted 10 March 2021; published 12 May 2021)

The standard model of spin-transfer torque (STT) in antiferromagnetic spintronics considers the exchange of angular momentum between quantum spins of flowing electrons and noncollinear-to-them localized spins treated as *classical* vectors. These vectors are assumed to realize Néel order in equilibrium, $\uparrow\downarrow\cdots\uparrow\downarrow$, and their STT-driven dynamics is described by the Landau-Lifshitz-Gilbert (LLG) equation. However, many experimentally employed materials (such as archetypal NiO) are strongly electron-correlated antiferromagnetic Mott insulators (AFMIs) whose localized spins form a ground state quite different from the unentangled Néel state $|\uparrow\downarrow\cdots\uparrow\downarrow\rangle$. The true ground state is entangled by quantum spin fluctuations, leading to the expectation value of all localized spins being *zero*, so that LLG dynamics of classical vectors of fixed length rotating due to STT cannot even be initiated. Instead, a fully quantum treatment of *both* conduction electrons and localized spins is necessary to capture the exchange of spin angular momentum between them, denoted as *quantum STT*. We use a recently developed time-dependent density matrix renormalization group approach to quantum STT to predict how injection of a spin-polarized current pulse into a normal metal layer coupled to an AFMI overlayer via exchange interaction and possibly small interlayer hopping—mimicking, e.g., topological-insulator/NiO bilayer employed experimentally—will induce a nonzero expectation value of AFMI localized spins. This new nonequilibrium phase is a spatially inhomogeneous ferromagnet with a zigzag profile of localized spins. The total spin absorbed by AFMI increases with electron-electron repulsion in AFMIs, as well as when the two layers do not exchange any charge.

DOI: 10.1103/PhysRevLett.126.197202

Introduction.—The emergence of antiferromagnetic spintronics [1–4] has elevated antiferromagnetic (AF) insulators (AFIs) and metals into active elements of spintronic devices. They exhibit dynamics of their localized spins at much higher frequencies, reaching THz [4], when compared to ferromagnetic spintronics. Furthermore, the absence of net magnetization forbids any stray magnetic fields, making them largely insensitive to perturbations by external fields. They also exhibit magnetoresistance effects [5,6] enabling the electric readout of changes in the orientations of their localized spins.

Basic spintronic phenomena like spin-transfer torque (STT) [7–10], where spin angular momentum is exchanged between flowing conduction electrons and noncollinear-to-them [11] localized spins; and spin pumping [12], where precessing localized spins pump pure spin current in the absence of any bias voltage, have been demonstrated recently using different AF materials. The theoretical description [13–22] of these phenomena invariably assumes that localized magnetic moments on two sublattices of the AF material, $\mathbf{M}_i^A$ and $\mathbf{M}_i^B$, are *classical* vectors with net zero total magnetization in equilibrium due to the assumed Néel classical ground state (GS), $\uparrow\downarrow\cdots\uparrow\downarrow$. Out of equilibrium, the dynamics of such classical vectors of fixed length is described by the Landau-Lifshitz-Gilbert (LLG) equation [23]. The STT is typically introduced into the LLG equation either as a phenomenological term [17–20], or it is calculated microscopically by using steady-state single-particle quantum transport formalism applied to model [13,14,21] or first-principles [15,16,22] Hamiltonians of AF materials. Recently STT [24] from time-dependent single-particle quantum transport formalism [25] has been coupled [26] to the LLG equation, capturing additional quantum effects like electronic spin pumping by moving $\mathbf{M}_i^A(t)$ and $\mathbf{M}_i^B(t)$ and the corresponding enhanced damping on them, but this remains the conventional [11] *quantum*-for-electrons–*classical*-for-localized-spins approach to STT.

However, AFIs employed in spintronics experiments are typically strongly electron-correlated transition metal oxides due to narrow *d* bands. For example, widely used [6–10] NiO shares features of both Mott and charge-transfer insulators [27–30]. Because of quantum (or zero-point) spin fluctuations [31–33], the AF GS is highly *entangled* [32–36], which results in a *zero* expectation value of all localized spins, $\mathbf{S}_i = 0$ (so, $\mathbf{M}_i^{A,B} \propto \mathbf{S}_i^{A,B} = 0$). Thus, conventional [11] STT $\propto \mathbf{s}_i \times \mathbf{S}_i = 0$ due to injected nonequilibrium electronic spin density $\mathbf{s}_i$ *cannot* be initiated because $\mathbf{S}_i(t=0) \equiv 0$. Even if $|\mathbf{S}_i(t=0)| \neq 0$ is provoked by spin-rotation-symmetry-breaking anisotropies

[37] or impurities [see Supplemental Material (SM) [38] for illustration], the LLG equation is inapplicable [40,41] because the length $|\mathbf{S}_i(t)| < |\mathbf{S}_i^{\mathrm{Neel}}|$ will be changing in time, with a smaller value signifying higher entanglement (unobserved quantum systems exhibit unitary evolution toward states of higher entanglement [42]). Thus, both situations necessitate to describe localized spins fully quantum mechanically where their expectation values $\mathbf{S}_i(t)$ *are calculated only at the end*.

The entanglement in the AF GS leading to $\mathbf{S}_i = 0$ can be illustrated using a one-dimensional (1D) quantum spin-$\frac{1}{2}$ Heisenberg AF chain [43,44] as the simplest example of an AFI defined on N_{AFI} sites:

$$\hat{H}_{\mathrm{AFI}} = J \sum_{i=1}^{N_{\mathrm{AFI}}-1} \hat{\mathbf{S}}_i \cdot \hat{\mathbf{S}}_{i+1}. \tag{1}$$

Here $\hat{S}_i^\alpha = \hat{I}_1 \otimes \cdots \otimes \frac{1}{2}\hat{\sigma}^\alpha \otimes \cdots \otimes \hat{I}_{N_{\mathrm{AFI}}}$ acts nontrivially, as the Pauli matrix $\hat{\sigma}^\alpha$, only on the Hilbert space of site i; $\hat{I}_i$ is the unit operator; and $J > 0$ is the AF exchange interaction. The true GS is easy to write explicitly for small N_{AFI}, such as for $N_{\mathrm{AFI}} = 4$ we find $|\mathrm{GS}\rangle = \frac{1}{\sqrt{12}}(2|\uparrow\downarrow\uparrow\downarrow\rangle + 2|\downarrow\uparrow\downarrow\uparrow\rangle - |\uparrow\uparrow\downarrow\downarrow\rangle - |\uparrow\downarrow\downarrow\uparrow\rangle - |\downarrow\downarrow\uparrow\uparrow\rangle - |\downarrow\uparrow\uparrow\downarrow\rangle)$. Its energy, $\langle \mathrm{GS}|\hat{H}_{\mathrm{AFI}}|\mathrm{GS}\rangle = -2J$, is lower than the energy of the unentangeled (i.e., direct-product) Néel state, $\langle\uparrow\downarrow\uparrow\downarrow|\hat{H}_{\mathrm{AFI}}|\uparrow\downarrow\uparrow\downarrow\rangle = -J$. This is in sharp contrast to ferromagnets where quantum spin fluctuations are absent, and both classical $\uparrow\uparrow\cdots\uparrow\uparrow$ and its unentangled quantum counterpart $|\uparrow\uparrow\cdots\uparrow\uparrow\rangle$ are the GS of the respective classical and quantum Hamiltonians [such as Eq. (1) with $J < 0$]. This justifies [40,41] the picture of interacting classical $\mathbf{M}_i$ in spintronics [11] and micromagnetics [23], even as the size of the localized spin is reduced to that of a single electron spin. Conversely, in the case of a many-body entangled [32–36] AF GS, the quantum state of each localized spin subsystem *must* be described by the reduced density matrix, $\hat{\rho}_i = \mathrm{Tr}_{\mathrm{other}}|\mathrm{GS}\rangle\langle\mathrm{GS}|$, where partial trace is performed in the Hilbert subspace of all other localized spins $j \neq i$. The expectation value

$$\mathbf{S}_i \equiv \langle\hat{\mathbf{S}}_i\rangle = \mathrm{Tr}[\hat{\rho}_i\hat{\mathbf{S}}_i] \tag{2}$$

is then identically a zero vector, $\mathbf{S}_i = 0$, on all sites (see the SM [38]). The GS in the limit $N_{\mathrm{AFI}} \to \infty$ is computable by the Bethe ansatz [44], and its entanglement ensures $\mathbf{S}_i = 0$. The entanglement in the GS of the crystalline realization of 1D [45] and two-dimensional (2D) [36] quantum Heisenberg antiferromagnets, as well as of an AF Mott insulator (AFMI) [46] realized with cold atoms on a square lattice, has been detected by neutron scattering or optically, respectively, at ultralow temperatures.

In this Letter, we employ the emerging concept of quantum STT [47–50] where both conduction electrons and localized spins are treated fully quantum mechanically to describe the exchange of spin angular momentum between them. This allows us to predict the nonequilibrium phase transition of an AFMI driven by the absorption of spin angular momentum from the spin-polarized current pulse injected into an adjacent normal metal (NM). To model such a genuine quantum many-body problem, we evolve in time a nonequilibrium quantum state of NM/AFMI system via the very recently adapted [49] to quantum STT time-dependent density matrix renormalization group (TDMRG) approach [51–55].

Our system geometry in Fig. 1 consists of a NM modeled as a 1D tight-binding (TB) chain, which is split into the left

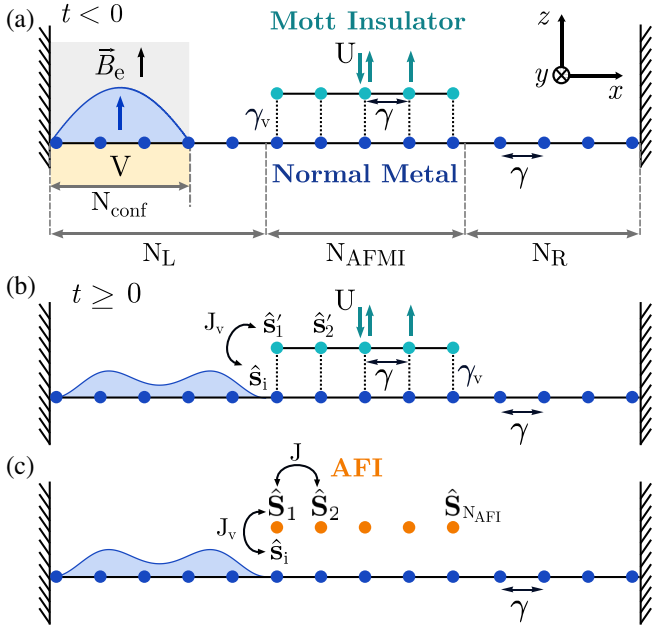

FIG. 1. (a) Schematic view of a "bilayer" [10] for TDMRG calculations. The 1D TB chain (blue dots) of $N = N_L + N_{\mathrm{AFMI}} + N_R = 92$ sites, with intrachain hopping γ, models the metallic surface (such as that of topological insulator Bi_2Se_3 in the experiments of Ref. [10]) through which a spin-polarized current pulse is injected. The pulse exerts quantum STT on a Hubbard chain of $N_{\mathrm{AFMI}} = 12$ sites with the on-site Coulomb repulsion U, modeling the surface of a strongly electron-correlated AFMI (such as that of NiO in Refs. [7–10]). The electronic spins in two chains interact via interchain exchange interaction J_v, and we consider both $\gamma_v = 0$ and $\gamma_v \neq 0$ interchain hopping where the latter mimics possible hybridization of a NM and AFMI via evanescent wave functions [22]. For times $t < 0$, $N_e = 12$ noninteracting electrons are confined by potential V within $N_{\mathrm{conf}} = 25$ sites of the L lead (composed of $N_L = 40$ sites), as well as spin-polarized by an external magnetic field $\mathbf{B}_e$ along the z axis. Concurrently, $N_e^{\mathrm{AFMI}} = 12$ electrons half-fill the AFMI chain. For times $t \geq 0$, V and $\mathbf{B}_e$ are removed, so that electrons propagate as a spin-polarized current pulse from the L to the R lead, as animated in the movie in the SM [38]. In panel (c), the AFMI from (a) and (b) is replaced by an AFI modeled as a quantum Heisenberg AF chain whose spin-$\frac{1}{2}$ operators reside on each (orange) site and interact via $J = 4\gamma^2/U$ in Eq. (1) while no electrons are allowed within this chain.

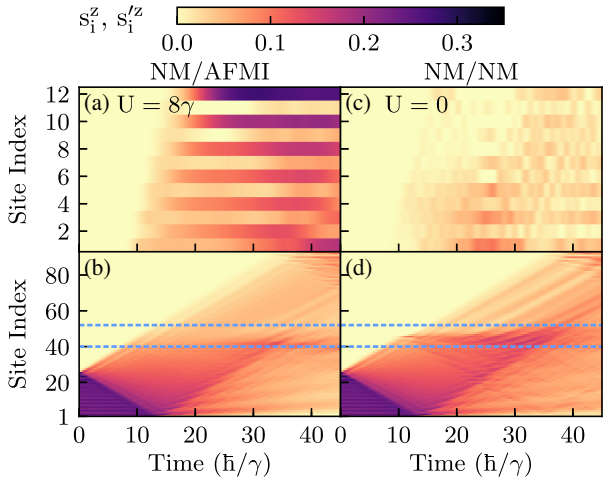

FIG. 2. Spatiotemporal profiles of the z component of spin density within: (a) an AFMI chain with the Coulomb repulsion $U = 8\gamma$; and (c) the same chain with $U = 0$ (acting then as the second NM chain half-filled with electrons). In both panels $s_i'^z(t = 0) \equiv 0$, so that only the $s_i'^z(t) \neq 0$ component is induced by a current pulse spin-polarized along the z axis and flowing along the bottom NM chain in Fig. 1(b) whose s_i^z profiles in panels (b) and (d) are driving the profiles in panels (a) and (c), respectively, via quantum STT. The dotted horizontal lines in (b) and (d) mark the boundaries between the leads and the central region of the NM chain in Fig. 1. The interchain exchange is $J_v = 0.5\gamma$ and hopping $\gamma_v = 0$ in Eq. (5). All four panels, together with the corresponding electron densities, are animated in the movie in the SM [38].

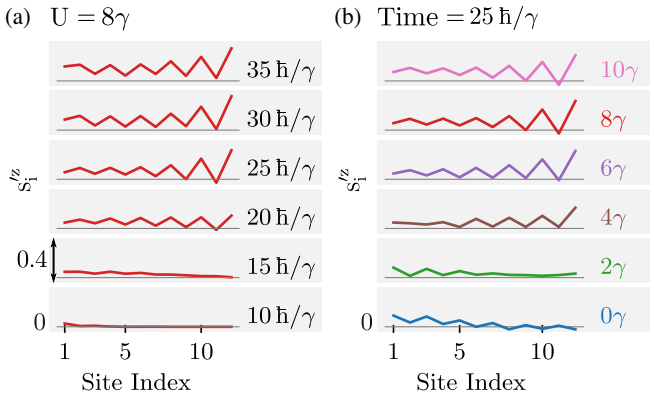

FIG. 3. Spatial profile of the z component $s_i'^z$ of the spin density within the AFMI chain in Fig. 1(b) driven by quantum STT from the NM chain: (a) at different times using $U = 8\gamma$ in Eq. (4); and (b) for different U values at time $t = 25\hbar/\gamma$. The interchain exchange is $J_v = 0.5\gamma$ and hopping $\gamma_v = 0$ in Eq. (5).

(L) and the right (R) leads sandwiching a central region. The conduction electron spins in the central region are exchange coupled to an AFMI chain modeled by the Hubbard model with the on-site Coulomb repulsion U. The current pulse, carrying electrons initially spin polarized in the direction perpendicular to the interface (i.e., along the z axis in Fig. 1), is injected from the L lead into the central region of the NM in order to initiate the AFMI dynamics via quantum STT. Our geometry mimics the recent experiment [10] on the injection of current pulses into the metallic surface of a topological insulator Bi_2Se_3, which then exert spin torque on the surface of a NiO overlayer covering Bi_2Se_3, except that in the experiment spin-orbit coupling polarizes injected electrons in the plane of the interface (i.e., along the y axis in Fig. 1). Nevertheless, since the singlet with $\mathbf{s}_i'(t = 0) \equiv 0$ on all sites of an AFMI is rotationally invariant, the final spin state of an AFMI driven by quantum STT will be the same for the arbitrary spin polarization of injected electrons.

Our *main* results in Figs. 2–5 demonstrate how quantum STT deposits spin angular momentum [Figs. 4 and 5] into the AFMI by driving its on-site electronic spin expectation value from $\mathbf{s}_i'(t = 0) \equiv 0$ in equilibrium toward the spatially inhomogeneous profile [Figs. 2(a) and 3], $s_i'^z(t) \neq 0$ $[s_i'^x(t) = 0 = s_i'^y(t)]$ with a zigzag pattern $s_{2j-1}'^z(t) < s_{2j}'^z(t)$ for $j = 1, \ldots, N_{\mathrm{AFMI}}/2$. The total spin angular momentum absorbed by the AFMI increases with the on-site Coulomb repulsion [Fig. 5(a)], but it is reduced [Figs. 4(c)] when the interchain hopping allows for hybridization of the NM and the AFMI, and electron leakage from the AFMI [Fig. 4(a)] into NM [Fig. 4(b)]. Prior to delving into the results, we introduce notation and concepts.

Models and methods.—The second-quantized many-electron Hamiltonian describing the NM/AFMI system in Fig. 1(a) consists of four terms:

$$\hat{H} = \hat{H}_{\mathrm{NM}} + \hat{H}_{\mathrm{AFMI}} + \hat{H}_{\mathrm{NM-AFMI}} + \hat{H}_{V,\mathbf{B}}(t < 0). \quad (3)$$

The first term is the 1D TB Hamiltonian of noninteracting electrons within the NM chain $\hat{H}_{\mathrm{NM}} = -\gamma \sum_{i=1}^{N} (\hat{c}_{i\uparrow}^{\dagger}\hat{c}_{i+1\uparrow} + \hat{c}_{i\downarrow}^{\dagger}\hat{c}_{i+1\downarrow} + \mathrm{H.c.})$ where $\hat{c}_{i\sigma}^{\dagger}$ ($\hat{c}_{i\sigma}$) creates (annihilates) an electron with spin $\sigma = \uparrow, \downarrow$ at site i, and γ is the intrachain hopping. These operators act on four possible states at each site i—vacuum $|0\rangle$, spin-up $|\uparrow\rangle$, spin-down $|\downarrow\rangle$, and doubly occupied state $|\uparrow\downarrow\rangle$, so that the total Hilbert space of the NM/AFMI system has dimension $4^{92} \times 4^{12}$. The interacting electrons within the AFMI chain are described by the Hubbard Hamiltonian [43,44]

$$\hat{H}_{\mathrm{AFMI}} = -\gamma \sum_{i=1}^{N_{\mathrm{AFMI}}-1} (\hat{d}_{i\uparrow}^{\dagger}\hat{d}_{i+1\uparrow} + \hat{d}_{i\downarrow}^{\dagger}\hat{d}_{i+1\downarrow} + \mathrm{H.c.}) + U \sum_{i=1}^{N_{\mathrm{AFMI}}} \hat{n}_{i\uparrow}'\hat{n}_{i\downarrow}'. \quad (4)$$

Here, $\hat{n}_{i\sigma}' = \hat{d}_{i\sigma}^{\dagger}\hat{d}_{i\sigma}$ is electron density (per site) operator for spin σ at site i of the AFMI. The on-site Coulomb repulsion, such as $U = 0$–10γ in Fig. 3(b), is expressed in the units of hopping γ (typically $\gamma = 1$ eV) which we use

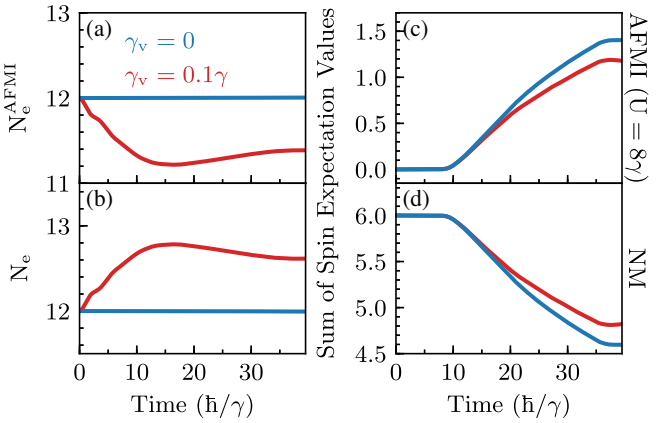

FIG. 4. Time dependence of the total number of electrons within (a) an AFMI and (b) NM chains in the setup of Fig. 1(b) for two different interchain hoppings $\gamma_v = 0$ (blue lines) and $\gamma_v = 0.1\gamma$ (red lines). Panels (c) and (d) show the corresponding time dependence of the sum of the z component of spin densities, $\sum_i s_i'^z$ and $\sum_i s_i^z$, respectively. The on-site Coulomb repulsion is $U = 8\gamma$ [Eq. (4)] within the AFMI and the interchain exchange is $J_v = 0.5\gamma$.

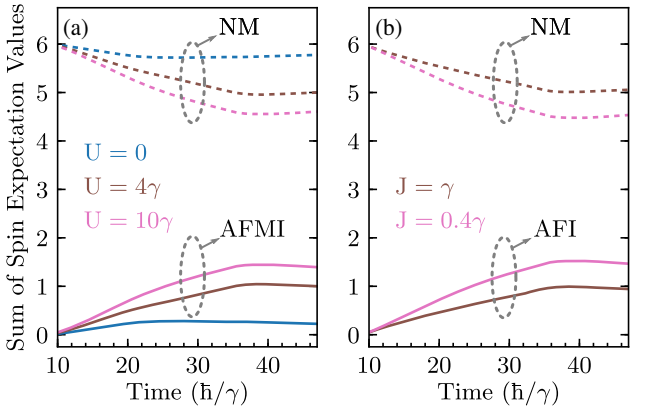

FIG. 5. (a) Time evolution of the sum of spin densities within the NM chain $\sum_i s_i^z$ (dashed lines) and AFMI chain $\sum_i s_i'^z$ (solid lines) in the setup of Fig. 1(b) for different values of the on-site Coulomb repulsion U within the AFMI chain. For comparison, panel (b) plots the same information for the setup in Fig. 1(c) where the AFMI is replaced by the AFI, modeled by the quantum spin-$\frac{1}{2}$ Heisenberg AF chain with no electrons, so that solid lines are $\sum_i S_i^z$ where S_i^z is obtained from Eq. (2). For each U in (a), we set the corresponding intrachain exchange interaction J [Eq. (1)] within the AFI in (b) as $J = 4\gamma^2/U$. The interchain exchange is $J_v = 0.5\gamma$.

as a unit of energy. The operators for the total number of electrons, $\hat{N}_e^{\mathrm{AFMI}} = \sum_i \hat{n}_i'$, and total spin along the α axis, $\hat{s}'^{\alpha} = \sum_i \hat{s}_i'^{\alpha}$, are given by the sum of electron and spin density operators, $\hat{n}_i' = \sum_{\sigma=\{\uparrow,\downarrow\}} \hat{d}_{i\sigma}^{\dagger}\hat{d}_{i\sigma}$ and $\hat{s}_i'^{\alpha} = \sum_{\sigma,\sigma'=\{\uparrow,\downarrow\}} \hat{d}_{i\sigma}^{\dagger} \frac{1}{2}\hat{\sigma}_{\sigma\sigma'}^{\alpha}\hat{d}_{i\sigma'}$, respectively. The interchain exchange interaction J_v between electronic spins within the NM and AFMI is described by

$$\hat{H}_{\text{NM-AFMI}} = -J_v \sum_{i=1}^{N_{\mathrm{AFMI}}} \hat{\mathbf{s}}_{i+N_L} \cdot \hat{\mathbf{s}}_i' - \gamma_v \sum_{i=1}^{N_{\mathrm{AFMI}}} (\hat{c}_{i+N_L\uparrow}^{\dagger}\hat{d}_{i\uparrow} + \hat{c}_{i+N_L\downarrow}^{\dagger}\hat{d}_{i\downarrow} + \text{H.c.}), \tag{5}$$

where $\hat{\mathbf{s}}_i$ and $\hat{\mathbf{s}}_i'$ are spin density (per site) operators in NM and AFMI chains, respectively. Here we also add a term with possible $\gamma_v \neq 0$ hopping between N_{AFMI} sites of the central region of the NM chain and N_{AFMI} sites of the AFMI in Fig. 1(a), which can arise in realistic devices used in spintronics [7–10] due to evanescent wave functions [22]. They penetrate from the NM surface into the region of the AFMI near the interface, thereby leading to charge transfer in equilibrium or current leakage between the two materials [22]. Such a normal-metal proximity effect on finite-size Mott insulators can also create exotic many-body states in equilibrium [56]. To prepare the initial state of the conduction electrons in the NM chain, we confine them within N_{conf} sites of the L lead in Fig. 1(a) and polarize their spins along the $+z$ axis by means of an additional term $\hat{H}_{V,\mathbf{B}}(t<0) = -V\sum_{i=1}^{N_{\mathrm{conf}}}(\hat{c}_{i\uparrow}^{\dagger}\hat{c}_{i\uparrow} + \hat{c}_{i\downarrow}^{\dagger}\hat{c}_{i\downarrow}) - \sum_{i=1}^{N_{\mathrm{conf}}} g\mu_B \hat{s}_i^z B_e^z$.

Here $V = 2.5\gamma$ is the confining potential; B_e^z is the external magnetic field; and $g\mu_B B_e^z = 10\gamma$, where g is the electron gyromagnetic ratio, and μ_B is the Bohr magneton. After the initial state is prepared for $t < 0$, $\hat{H}_{V,\mathbf{B}}(t \geq 0)$ is set to zero, so that spin-polarized electrons from the L lead propagate toward the R lead, as illustrated in Fig. 1(b), computed in Fig. 2, and animated in the SM [38].

In the limit $U \gg \gamma$, the half-filled ($n_i = 1$) 1D Hubbard model describes electrons localized one per site, so it can be mapped [43,44] to an isotropic quantum spin-$\frac{1}{2}$ Heisenberg AF chain with the effective Hamiltonian given in Eq. (1). Therefore, for comparison we also analyze the NM/AFI setup in Fig. 1(c) where AFI sites host localized spin-$\frac{1}{2}$ operators $\hat{\mathbf{S}}_i$, as described by the Hamiltonian $\hat{H} = \hat{H}_{\mathrm{NM}} + \hat{H}_{\mathrm{AFI}} + \hat{H}_{\mathrm{NM-AFI}} + \hat{H}_{V,\mathbf{B}}(t<0)$. Here $\hat{H}_{\mathrm{NM}}$ is the same as in Eq. (3); $\hat{H}_{\mathrm{AFI}}$ is the same as in Eq. (1) where we use $J = 4\gamma^2/U$ as the exchange interaction in the limit $U \gg \gamma$ [43,44]; the interchain interaction is described by $\hat{H}_{\mathrm{NM-AFI}} = -J_v \sum_{i=1}^{N_{\mathrm{AFI}}} \hat{\mathbf{s}}_{i+N_L} \cdot \hat{\mathbf{S}}_i$ where $J_v = 0.5\gamma$; and $\hat{H}_{V,\mathbf{B}}(t<0)$ is the same as in Eq. (3).

The TDMRG simulations [51–55] evolve the nonequilibrium state of the whole system in Fig. 1, $|\Psi(t+\delta t)\rangle = e^{-i\hat{H}\delta t/\hbar}|\Psi(t)\rangle$, using the time step $\delta t = 0.1\hbar/\gamma$. Additional details of TDMRG simulations are provided in the SM [38].

Results and discussion.—The Hubbard 1D chain modeling the AFMI possesses a sizable energy gap Δ_c for charge excitations at $U \gtrsim 2\gamma$, whose value is exactly known [44] in the limit $N_{\mathrm{AFMI}} \to \infty$ ($\Delta_c = 0.173\gamma$ at $U = 2\gamma$; or $\Delta_c = 0.631\gamma$ at $U = 3\gamma$). In chains of finite length, such as ours

with $N_{\mathrm{AFMI}} = 12$ sites, the DMRG predicts slightly larger Δ_c values [57]. However, the spin sector of the half-filled Hubbard chain is gapless in the thermodynamic limit. This means that injecting a charge in the AFMI is energetically costly, but creating a spin excitation is not. Figures 2(a) and 3 demonstrate that the AFMI with $U \gtrsim 4\gamma$ will be driven out of its GS with $\mathbf{s}'_i = 0$ on all sites toward a nonequilibrium phase with $s'^z_i(t) \neq 0$ and $s'^x_i = 0 = s'^y_i$ due to quantum STT exerted by the injected current pulse in the NM chain that is spin polarized along the z axis. The spatial profile of $s'^z_i(t)$ is inhomogeneous with a zigzag pattern deep in the Mott insulator phase, which distinguishes it from the weak response of the borderline case with $U = 2\gamma$ [Fig. 3(b)] or the noninteracting chain with $U = 0$ [Figs. 2(c) and 3(b)].

Even after the current pulse in the NM chain has ended, the spin angular momentum remains deposited within the AFMI, with its total value increasing with U [Fig. 5(a)]. Such a Mott insulator transmuted into a phase with nonzero total magnetization remains magnetized also when intrachain hopping is switched on, $\gamma_v = 0.1\gamma$, in Fig. 4(c). However, $\gamma_v = 0.1\gamma$ allows electrons to leak from the AFMI [Fig. 4(a)] into the NM [Fig. 4(b)] chain, so that the total spin deposited into the AFMI is reduced in Fig. 4(c) when compared to the isolated AFMI.

Figure 5 explains quantum STT [47–50] as the transfer of total spin angular momentum from NM conduction electrons (dashed lines in Fig. 5) to confined electrons within the AFMI [solid lines in Fig. 5(a)] or to localized spins within the AFI [solid lines in Fig. 5(b)]. While some spin transfer exists even for $U = 0$, it is dramatically enhanced by increasing U to establish the AFMI [Fig. 5(a)]. The NM/AFMI case with $U = 10\gamma$ shows that $\sum_i s'^z_i(t)$ within the AFMI is nearly identical to $\sum_i S^z_i(t)$ within the AFI with $J = 4\gamma^2/U$, as anticipated from mapping [43,44] of the AFMI to the AFI in the limit $U \gg \gamma$. However, this correspondence fails for $U < 10\gamma$. The absorbed spin by the AFMI or AFI can be viewed as multiple excitations of any two-spinon or higher-order spinon states [58], as long as they are compatible with total angular momentum conservation [49].

Conclusions.—In conclusion, we demonstrate how the TDMRG approach [51–55] adapted [49] for quantum STT [47–50] makes it possible to study spin transfer into strongly electron-correlated antiferromagnets. In contrast, quantum-classical theory of conventional STT [11,13–22] would conclude that an entangled AF true GS does not undergo any current-driven dynamics when its localized spins have zero expectation value at $t = 0$ as the initial state used in this study. Although the TDMRG approach has been previously applied to study the charge current through an AFMI [59–61] or spin-charge separation [62] in geometries where electrons are injected into the AFMI by finite bias voltage, spin-dependent transport phenomena in geometries like Fig. 1 of relevance to spintronics [7–10] remain unexplored. Realistic spintronic devices would require us to consider 2D or 3D geometries. But Keldysh Green functions [25,63], as the only available nonequilibrium quantum many-body formalism for higher dimensions and longer times, cannot at present access large U with perturbative self-energies [57,63], or its nonperturbative implementation can handle [64] only a very few sites. Therefore, this study represents a pivotal test case that provides intuition about quantum STT phenomena in strongly correlated and/or entangled quantum materials, as well as a benchmark [63] for any future developments via the Keldysh Green functions.

M. D. P., P. M., and B. K. N. were supported by the U.S. National Science Foundation (NSF) Grant No. ECCS 1922689. A. E. F. was supported by the U.S. Department of Energy (DOE) Grant No. DE-SC0019275.

Note added in the proof.—Recently, we became aware of Ref. [65] in which quantum spin torque on 1D quantum spin-$\frac{1}{2}$ Heisenberg AF chain was studied due to injection of single-electron spin-polarized current pulse, which (as a special case) is in accord with our results in Fig. 5(b) where multielectron spin-polarized current pulse is used.

*bnikolic@udel.edu

[1] V. Baltz, A. Manchon, M. Tsoi, T. Moriyama, T. Ono, and Y. Tserkovnyak, Antiferromagnetic spintronics, Rev. Mod. Phys. **90**, 015005 (2018).
[2] T. Jungwirth, X. Marti, P. Wadley, and J. Wunderlich, Antiferromagnetic spintronics, Nat. Nanotechnol. **11**, 231 (2016).
[3] J. Železný, P. Wadley, K. Olejník, A. Hoffman, and H. Ohno, Spin transport and spin torque in antiferromagnetic devices, Nat. Phys. **14**, 220 (2018).
[4] B. Jungfleisch, W. Zhang, and A. Hoffmann, Perspectives of antiferromagnetic spintronics, Phys. Lett. A **382**, 865 (2018).
[5] A. Manchon, Spin Hall magnetoresistance in antiferromagnet/normal metal bilayers, Phys. Status Solidi RRL **11**, 1600409 (2017).
[6] L. Baldrati *et al.*, Full angular dependence of the spin Hall and ordinary magnetoresistance in epitaxial antiferromagnetic NiO(001)/Pt thin films, Phys. Rev. B **98**, 024422 (2018).
[7] X. Z. Chen *et al.*, Antidamping-Torque-Induced Switching in Biaxial Antiferromagnetic Insulators, Phys. Rev. Lett. **120**, 207204 (2018).
[8] T. Moriyama, K. Oda, T. Ohkochi, M. Kimata, and T. Ono, Spin torque control of antiferromagnetic moments in NiO, Sci. Rep. **8**, 14167 (2018).
[9] I. Gray *et al.*, Spin Seebeck Imaging of Spin-Torque Switching in Antiferromagnetic Pt/NiO Heterostructures, Phys. Rev. X **9**, 041016 (2019).
[10] Y. Wang *et al.*, Magnetization switching by magnon-mediated spin torque through an antiferromagnetic insulator, Science **366**, 1125 (2019).

[11] D. Ralph and M. Stiles, Spin transfer torques, J. Magn. Magn. Mater. **320**, 1190 (2008).

[12] P. Vaidya, A. Morley, J. van Tol, Y. Liu, R. Cheng, A. Brataas, D. Lederman, and E. del Barco, Subterahertz spin pumping from an insulating antiferromagnet, Science **368**, 160 (2020).

[13] A. S. Núñez, R. A. Duine, P. Haney, and A. H. MacDonald, Theory of spin torques and giant magnetoresistance in antiferromagnetic metals, Phys. Rev. B **73**, 214426 (2006).

[14] P. M. Haney and A. H. MacDonald, Current-Induced Torques Due to Compensated Antiferromagnets, Phys. Rev. Lett. **100**, 196801 (2008).

[15] Y. Xu, S. Wang, and K. Xia, Spin-Transfer Torques in Antiferromagnetic Metals from First Principles, Phys. Rev. Lett. **100**, 226602 (2008).

[16] M. Stamenova, R. Mohebbi, J. Seyed-Yazdi, I. Rungger, and S. Sanvito, First-principles spin-transfer torque in CuMnAs|GaP|CuMnAs junctions, Phys. Rev. B **95**, 060403(R) (2017).

[17] K. M. D. Hals, Y. Tserkovnyak, and A. Brataas, Phenomenology of Current-Induced Dynamics in Antiferromagnets, Phys. Rev. Lett. **106**, 107206 (2011).

[18] H. V. Gomonay and V. M. Loktev, Spin transfer and current-induced switching in antiferromagnets, Phys. Rev. B **81**, 144427 (2010).

[19] R. Cheng, J. Xiao, Q. Niu, and A. Brataas, Spin Pumping and Spin-Transfer Torques in Antiferromagnets, Phys. Rev. Lett. **113**, 057601 (2014).

[20] R. Cheng, M. W. Daniels, J.-G. Zhu, and D. Xiao, Ultrafast switching of antiferromagnets via spin-transfer torque, Phys. Rev. B **91**, 064423 (2015).

[21] H. B. M. Saidaoui, A. Manchon, and X. Waintal, Spin transfer torque in antiferromagnetic spin valves: From clean to disordered regimes, Phys. Rev. B **89**, 174430 (2014).

[22] K. Dolui, M. D. Petrović, K. Zollner, P. Plecháč, J. Fabian, and B. K. Nikolić, Proximity spin-orbit torque on a two-dimensional magnet within van der Waals heterostructure: Current-driven antiferromagnet-to-ferromagnet reversible nonequilibrium phase transition in bilayer CrI_3, Nano Lett. **20**, 2288 (2020).

[23] R. F. L. Evans, W. J. Fan, P. Chureemart, T. A. Ostler, M. O. A. Ellis, and R. W. Chantrell, Atomistic spin model simulations of magnetic nanomaterials, J. Phys. Condens. Matter **26**, 103202 (2014).

[24] A. Suresh, M. D. Petrović, H. Yang, and B. K. Nikolić, Magnon-Versus Electron-Mediated Spin-Transfer Torque Exerted by Spin Current Across an Antiferromagnetic Insulator to Switch the Magnetization of an Adjacent Ferromagnetic Metal, Phys. Rev. Applied **15**, 034089 (2021).

[25] B. Gaury, J. Weston, M. Santin, M. Houzet, C. Groth, and X. Waintal, Numerical simulations of time-resolved quantum electronics, Phys. Rep. **534**, 1 (2014).

[26] M. D. Petrović, B. S. Popescu, U. Bajpai, P. Plecháč, and B. K. Nikolić, Spin and Charge Pumping by a Steady or Pulse-Current-Driven Magnetic Domain Wall: A Self-Consistent Multiscale Time-Dependent Quantum-Classical Hybrid Approach, Phys. Rev. Applied **10**, 054038 (2018).

[27] M. Karolak, G. Ulm, T. Wehling, Y. Mazurenko, A. Poteryaev, and A. Lichtenstein, Double counting in LDA + DMFT-The example of NiO, J. Electron Spectrosc. Relat. Phenom. **181**, 11 (2010).

[28] F. Lechermann, W. Körner, D. F. Urban, and C. Elsässer, Interplay of charge-transfer and Mott-Hubbard physics approached by an efficient combination of self-interaction correction and dynamical mean-field theory, Phys. Rev. B **100**, 115125 (2019).

[29] S. Zhang, F. D. Malone, and M. A. Morales, Auxiliary-field quantum Monte Carlo calculations of the structural properties of nickel oxide, J. Chem. Phys. **149**, 164102 (2018).

[30] K. Gillmeister, D. Golež, C.-T. Chiang, N. Bittner, Y. Pavlyukh, J. Berakdar, P. Werner, and W. Widdra, Ultrafast coupled charge and spin dynamics in strongly correlated NiO, Nat. Commun. **11**, 4095 (2020).

[31] A. Singh and Z. Tešanović, Quantum spin fluctuations in an itinerant antiferromagnet, Phys. Rev. B **41**, 11457 (1990).

[32] S. Humeniuk, Quantum state tomography on a plaquette in the two-dimensional Hubbard model, Phys. Rev. B **100**, 115121 (2019).

[33] A. Kamra, E. Thingstad, G. Rastelli, R. A. Duine, A. Brataas, W. Belzig, and A. Sudbø, Antiferromagnetic magnons as highly squeezed Fock states underlying quantum correlations, Phys. Rev. B **100**, 174407 (2019).

[34] T. Roscilde, P. Verrucchi, A. Fubini, S. Haas, and V. Tognetti, Entanglement and Factorized Ground States in Two-Dimensional Quantum Antiferromagnets, Phys. Rev. Lett. **94**, 147208 (2005).

[35] O. Vafek, N. Regnault, and B. A. Bernevig, Entanglement of exact excited eigenstates of the Hubbard model in arbitrary dimension, SciPost Phys. **3**, 043 (2017).

[36] N. B. Christensen, H. M. Rønnow, D. F. McMorrow, A. Harrison, T. G. Perring, M. Enderle, R. Coldea, L. P. Regnault, and G. Aeppli, Quantum dynamics and entanglement of spins on a square lattice, Proc. Natl. Acad. Sci. U.S.A. **104**, 15264 (2007).

[37] E. M. Stoudenmire and S. R. White, Studying two-dimensional systems with the density matrix renormalization group, Annu. Rev. Condens. Matter Phys. **3**, 111 (2012).

[38] See Supplemental Material at http://link.aps.org/supplemental/10.1103/PhysRevLett.126.197202, which includes Ref. [39], for: (i) movie animating time evolution of spin densities, $s_i'^z(t)$ and $s_i^z(t)$, from Fig. 2, as well as time evolution of electron densities, $n_i'^z(t)$ and $n_i^z(t)$, within upper and lower chains in Fig. 1 for the same two setups ($U = 8\gamma$ and $U = 0$) used in Fig. 2; (*ii*) text with additional details of TDMRG simulations, as well as with one additional Figure showing spatial profiles of the expectation value [Eq. (2)] of spin operator $\mathbf{S}_i$ in both 1D and 2D quantum spin-$\frac{1}{2}$ Heisenberg antiferromagnets [Eq. (1)] which possess global spin rotation invariance or they contain a single symmetry-breaking impurity generating local magnetic field at one site.

[39] J. Gray, QUIMB: A Python library for quantum information and many-body calculations, J. Open Source Softw. **3**, 819 (2018).

[40] R. Wieser, Description of a dissipative quantum spin dynamics with a Landau-Lifshitz-Gilbert like damping and complete derivation of the classical Landau-Lifshitz equation, Eur. Phys. J. B **88**, 77 (2015).

[41] R. Wieser, Derivation of a time dependent Schrödinger equation as the quantum mechanical Landau-Lifshitz-Bloch equation, J. Phys. Condens. Matter **28**, 396003 (2016).

[42] B. Skinner, J. Ruhman, and A. Nahum, Measurement-Induced Phase Transitions in the Dynamics of Entanglement, Phys. Rev. X **9**, 031009 (2019).

[43] E. Fradkin, *Field Theories of Condensed Matter Physics* (Cambridge University Press, Cambridge, England, 2013).

[44] F. H. Essler, H. Frahm, F. Göhmann, A. Klümper, and V. E. Korepin, *The One-Dimensional Hubbard Model* (Cambridge University Press, Cambridge, England, 2005).

[45] S. Sahling, G. Remenyi, C. Paulsen, P. Monceau, V. Saligrama, C. Marin, A. Revcolevschi, L. P. Regnault, S. Raymond, and J. E. Lorenzo, Experimental realization of long-distance entanglement between spins in antiferromagnetic quantum spin chains, Nat. Phys. **11**, 255 (2015).

[46] A. Mazurenko, C. S. Chiu, G. Ji, M. F. Parsons, M. Kanász-Nagy, R. Schmidt, F. Grusdt, E. Demler, D. Greif, and M. Greiner, A cold-atom Fermi–Hubbard antiferromagnet, Nature (London) **545**, 462 (2017).

[47] A. Zholud, R. Freeman, R. Cao, A. Srivastava, and S. Urazhdin, Spin Transfer Due to Quantum Magnetization Fluctuations, Phys. Rev. Lett. **119**, 257201 (2017).

[48] P. Mondal, U. Bajpai, M. D. Petrović, P. Plecháč, and B. K. Nikolić, Quantum spin transfer torque induced nonclassical magnetization dynamics and electron-magnetization entanglement, Phys. Rev. B **99**, 094431 (2019).

[49] M. D. Petrović, P. Mondal, A. E. Feiguin, P. Plecháč, and B. K. Nikolić, Spintronics meets density matrix renormalization group: Quantum spin torque driven nonclassical magnetization reversal and dynamical buildup of long-range entanglement, arXiv:2002.04655 [Phys. Rev. X (to be published)].

[50] A. Mitrofanov and S. Urazhdin, Energy and momentum conservation in spin transfer, Phys. Rev. B **102**, 184402 (2020).

[51] S. R. White and A. E. Feiguin, Real-Time Evolution Using the Density Matrix Renormalization Group, Phys. Rev. Lett. **93**, 076401 (2004).

[52] P. Schmitteckert, Nonequilibrium electron transport using the density matrix renormalization group method, Phys. Rev. B **70**, 121302(R) (2004).

[53] A. J. Daley, C. Kollath, U. Schollwöck, and G. Vidal, Time-dependent density-matrix renormalization-group using adaptive effective Hilbert spaces, J. Stat. Mech. (2004) P04005.

[54] A. E. Feiguin, The density matrix renormalization group and its time-dependent variants, AIP Conf. Proc. **1419**, 5 (2011).

[55] S. Paeckel, T. Köhler, A. Swoboda, S. R. Manmana, U. Schollwöck, and C. Hubig, Time-evolution methods for matrix-product states, Ann. Phys. (Amsterdam) **411**, 167998 (2019).

[56] H. Zenia, J. K. Freericks, H. R. Krishnamurthy, and Th. Pruschke, Appearance of "Fragile" Fermi Liquids in Finite-Width Mott Insulators Sandwiched Between Metallic Leads, Phys. Rev. Lett. **103**, 116402 (2009).

[57] J.-P. Joost, N. Schlünzen, S. Hese, M. Bonitz, C. Verdozzi, P. Schmitteckert, and M. Hopjan, Löwdin's symmetry dilemma within Green functions theory for the one-dimensional Hubbard model, Contrib. Plasma Phys. e202000220 (2021).

[58] M. Mourigal, M. Enderle, A. Klöpperpieper, J.-S. Caux, A. Stunault, and H. M. Rønnow, Fractional spinon excitations in the quantum Heisenberg antiferromagnetic chain, Nat. Phys. **9**, 435 (2013).

[59] S. K. Irino and K. Ueda, Nonequilibrium current in the one dimensional Hubbard model at half-filling, J. Phys. Soc. Jpn. **79**, 093710 (2010).

[60] F. Heidrich-Meisner, I. González, K. A. Al-Hassanieh, A. E. Feiguin, M. J. Rozenberg, and E. Dagotto, Nonequilibrium electronic transport in a one-dimensional Mott insulator, Phys. Rev. B **82**, 205110 (2010).

[61] L. G. G. V. Dias da Silva, K. A. Al-Hassanieh, A. E. Feiguin, F. A. Reboredo, and E. Dagotto, Real-time dynamics of particle-hole excitations in Mott insulator-metal junctions, Phys. Rev. B **81**, 125113 (2010).

[62] T. Ulbricht and P. Schmitteckert, Is spin-charge separation observable in a transport experiment?, Europhys. Lett. **86**, 57006 (2009).

[63] N. Schlünzen, S. Hermanns, M. Scharnke, and M. Bonitz, Ultrafast dynamics of strongly correlated fermions-nonequilibrium Green functions and selfenergy approximations, J. Phys. Condens. Matter **32**, 103001 (2020).

[64] C. Bertrand, O. Parcollet, A. Maillard, and X. Waintal, Quantum Monte Carlo algorithm for out-of-equilibrium Green's functions at long times, Phys. Rev. B **100**, 125129 (2019).

[65] A. Mitrofanov and S. Urazhdin, Nonclassical Spin Transfer Effects in an Antiferromagnet, Phys. Rev. Lett. **126**, 037203 (2021).

Supplemental Material for "Quantum spin torque driven transmutation of antiferromagnetic Mott insulator"

Marko D. Petrović,[1] Priyanka Mondal,[1] Adrian E. Feiguin,[2] and Branislav K. Nikolić[1,*]

[1] *Department of Physics and Astronomy, University of Delaware, Newark DE 19716, USA*
[2] *Department of Physics, Northeastern University, Boston, MA 02115, USA*

In addition to the movie animating Fig. 2 in the main text, this Supplemental Material provides details of time-dependent (TDMRG) simulations, as well as one additional multi-panel Fig. S1 showing expectation value S_i^z of spin-$\frac{1}{2}$ operators, as defined in Eq. (2) of the main text, in the ground state (GS), $|\mathrm{GS}\rangle$, at each site i of either one-dimensional (1D) quantum spin-$\frac{1}{2}$ Heisenberg antiferromagnetic chain composed of $N_{\mathrm{AFI}} = 12$ sites [Figs. S1(a) and S1(b)] or two-dimensional (2D) quantum spin-$\frac{1}{2}$ Heisenberg antiferromagnet on 6×4 square lattice [Figs. S1(c) and S1(d)]. Both quantum spin systems are described by the quantum Heisenberg Hamiltonian [1, 2]

$$\hat{H}_{\mathrm{AFI}} = J \sum_{\langle i,j \rangle} \hat{\mathbf{S}}_i \cdot \hat{\mathbf{S}}_j - h\hat{S}_m^z, \tag{1}$$

as the simplest model of an antiferromagnetic insulator (AFI). Here the exchange interaction $J = 1$ eV is nonzero between the nearest-neighbor sites, as denoted by $\langle i, j \rangle$. Periodic boundary conditions are employed in both cases. The spin-$\frac{1}{2}$ operator at site i

$$\hat{S}_i^\alpha = \hat{I}_1 \otimes \ldots \otimes \frac{1}{2}\hat{\sigma}^\alpha \otimes \ldots \otimes \hat{I}_{\mathrm{N_{AFI}}}, \tag{2}$$

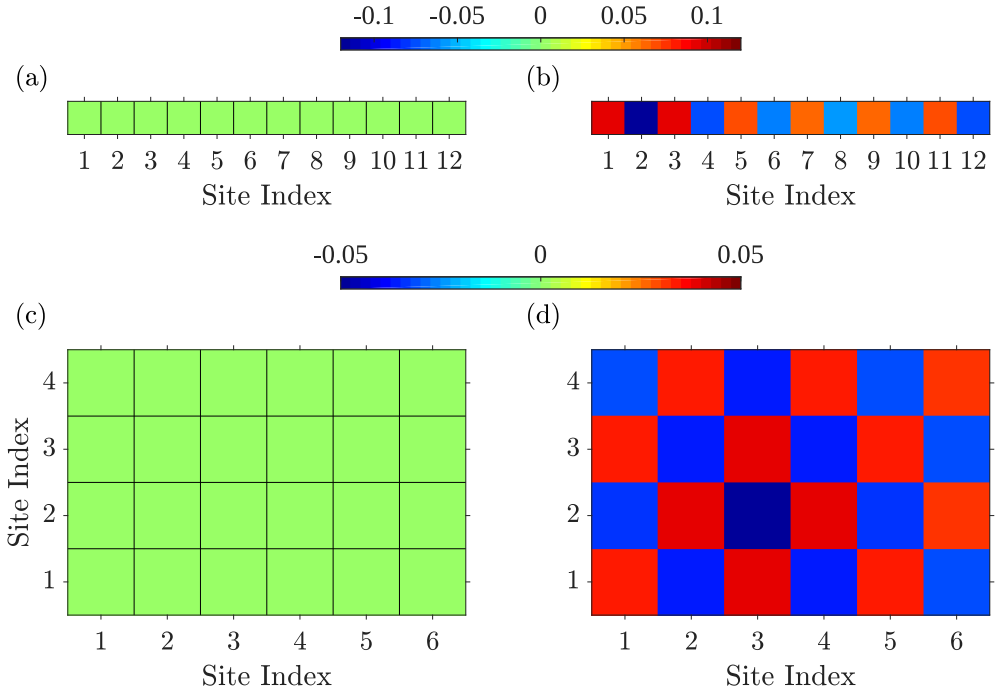

FIG. S1. Spatial profile of the z-component S_i^z [Eq. (2) in the main text] of spin operator in Eq. (2) within: (a) 1D chain of 12 sites described by the first term in Eq. (1); (b) 1D chain of 12 sites with the local magnetic field $h = 0.2J$ in the second term in Eq. (1) at site $m = 2$; (c) 2D square lattice described by the first term in Eq. (1); (d) 2D square lattice with the local magnetic field $h = 0.2J$ in the second term in Eq. (1) at site $m = (3, 2)$.

* bnikolic@udel.edu

acts nontrivially, as the Pauli matrix $\hat{\sigma}^{\alpha}$, only on the Hilbert space of site i; and $\hat{I}_i$ is the unit operator. We consider systems with the global spin rotation symmetry, as described by the first term only in Eq. (1); or we introduce an additional local magnetic field $h = 0.2J$ at site m of 1D or 2D lattice, due to, e.g., impurity whose spin is large and can be considered as a classical vector. The nonzero second term in Eq. (1) breaks the global spin rotation symmetry. The GS is found by exact diagonalization in 1D or in 2D by using QUIMB package [3].

One of the standard tools to quantify entanglement in many-body quantum systems is entanglement entropy of its subsystem [4], such as half of 1D chain or 2D lattice. We compute

$$\hat{\rho}_{\rm half} = {\rm Tr}_{\rm other-half} \, |{\rm GS}\rangle\langle{\rm GS}|, \tag{3}$$

and from it obtain the von Neumann entanglement entropy

$$S_{\rm half} = -{\rm Tr}\hat{\rho}_{\rm half} \log_2 \hat{\rho}_{\rm half}. \tag{4}$$

This entropy for systems in Fig. S1(a)–(d) is: (a) $S_{\rm half} = 1.71$; (b) $S_{\rm half} = 1.67$; (c) $S_{\rm half} = 2.96$; and (d) $S_{\rm half} = 2.91$, respectively. Thus, even though systems in Fig. S1(b) or Fig. S1(d) exhibit staggered pattern of expectation values S^z_i, akin to Néel classical ground state $\uparrow\downarrow \ldots \uparrow\downarrow$, their $|{\rm GS}\rangle$ remains highly entangled. This is also signified by $|\mathbf{S}_i| \ll |\mathbf{S}^{\rm N\acute{e}el}_i|$, where $|\mathbf{S}^{\rm N\acute{e}el}_i| = 1/2$ is for unentangled (i.e., separable or direct-product) Néel quantum state $|\uparrow\downarrow \ldots \uparrow\downarrow\rangle$.

The TDMRG simulations [5–9] in the main text evolve the nonequilibrium state of the whole system in Fig. 1 in the main text, $|\Psi(t+\delta t)\rangle = e^{-i\hat{H}\delta t/\hbar}|\Psi(t)\rangle$, using the time step $\delta t = 0.1\hbar/\gamma$. We start the propagation with $m = 100$ states and limit the truncation error to 10^{-7}, while the maximal number of states allowed during the evolution is set to $m_{\rm max} = 400$. Any single-particle expectation value at site i can be obtained from $\hat{\rho}_i(t) = {\rm Tr}_{\rm other} \, |\Psi(t)\rangle\langle\Psi(t)|$, as exemplified by Eq. (2) in the main text. Since fermionic leads are not semi-infinite as in usual quantum transport calculations [10], the systems in Fig. 1 in the main text can be evolved only for a limited time [11–14] before electrons are backscattered by the right boundary which breaks L→R current flow. For example, in Fig. 2 in the main text and its animation via the movie included as Supplemental Material, such backscattering occurs at $t \simeq 40\hbar/\gamma$. Nevertheless, the quantum dynamics of the conduction electrons in the NM chain and charge and spin confined within the AFMI chain can be safely assumed to be effectively equivalent to that in an infinite [10] open quantum system before the boundary reflection takes place.

[1] E. Fradkin, *Field Theories of Condensed Matter Physics* (Cambridge University Press, Cambridge, 2013).

[2] F. H. Essler, H. Frahm, F. Göhmann, A. Klümper, and V. E. Korepin, *The one-dimensional Hubbard model* (Cambridge University Press, Cambridge, 2005).

[3] J. Gray, QUIMB: A Python library for quantum information and many-body calculations, J. Open Source Softw. **3**, 819 (2018).

[4] O. Vafek, N. Regnault, and B. A. Bernevig, Entanglement of exact excited eigenstates of the Hubbard model in arbitrary dimension, SciPost Phys. **3**, 043 (2017).

[5] S. R. White and A. E. Feiguin, Real-time evolution using the density matrix renormalization group, Phys. Rev. Lett. **93**, 076401 (2004).

[6] P. Schmitteckert, Nonequilibrium electron transport using the density matrix renormalization group method, Phys. Rev. B **70**, 121302(R) (2004).

[7] A. J. Daley, C. Kollath, U. Schollwöck, and G. Vidal, Time-dependent density-matrix renormalization-group using adaptive effective Hilbert spaces, J. Stat. Mech: Theor. Exp. P04005 (2004).

[8] A. E. Feiguin, The density matrix renormalization group and its time-dependent variants, in A. Avella and F. Mancini (eds.), AIP Conference Proceedings **1419** (2011).

[9] S. Paeckel, T. Köhler, A. Swoboda, S. R. Manmana, U. Schollwöck, and C. Hubig, Time-evolution methods for matrix-product states, Ann. of Phys. **411**, 167998 (2019).

[10] M. D. Petrović, B. S. Popescu, U. Bajpai, P. Plecháč, and B. K. Nikolić, Spin and charge pumping by a steady or pulse-current-driven magnetic domain wall: A self-consistent multiscale time-dependent quantum-classical hybrid approach, Phys. Rev. Applied **10**, 054038 (2018).

[11] S. K. Irino and K. Ueda, Nonequilibrium current in the one dimensional Hubbard model at half-filling, J. Phys. Soc. Jpn. **79**, 093710 (2010).

[12] F. Heidrich-Meisner, I. González, K. A. Al-Hassanieh, A. E. Feiguin, M. J. Rozenberg, and E. Dagotto, Nonequilibrium electronic transport in a one-dimensional Mott insulator, Phys. Rev. B **82**, 205110 (2010).

[13] L. G. G. V. Dias da Silva, K. A. Al-Hassanieh, A. E. Feiguin, F. A. Reboredo, and E. Dagotto, Real-time dynamics of particle-hole excitations in Mott insulator-metal junctions, Phys. Rev. B **81**, 125113 (2010).

[14] T. Ulbricht and P. Schmitteckert, Is spin-charge separation observable in a transport experiment?, EPL (Europhysics Letters) **86**, 57006 (2009).